



## OPEN ACCESS

EDITED BY  
GM Shafiqullah,  
Murdoch University, Australia

REVIEWED BY  
Priya Ranjan Satpathy,  
Universiti Tenaga Nasional, Malaysia  
S. M. Ferdous,  
Murdoch University, Australia

\*CORRESPONDENCE  
Shiwei Xiao,  
✉ 1727325331@qq.com

RECEIVED 25 October 2025  
REVISED 03 February 2026  
ACCEPTED 25 February 2026  
PUBLISHED 18 March 2026

CITATION  
Xiao S (2026) Distributed robust  
optimization scheduling in  
multi-microgrids collaboration  
considering the participation of electric  
vehicles.  
*Front. Energy Res.* 14:1732386.  
doi: 10.3389/fenrg.2026.1732386

COPYRIGHT  
© 2026 Xiao. This is an open-access  
article distributed under the terms of  
the [Creative Commons Attribution  
License \(CC BY\)](https://creativecommons.org/licenses/by/4.0/). The use, distribution or  
reproduction in other forums is  
permitted, provided the original  
author(s) and the copyright owner(s) are  
credited and that the original  
publication in this journal is cited, in  
accordance with accepted academic  
practice. No use, distribution or  
reproduction is permitted which does  
not comply with these terms.

# Distributed robust optimization scheduling in multi-microgrids collaboration considering the participation of electric vehicles

Shiwei Xiao\*

School of Electrical Engineering, Shanghai University of Electric Power, Shanghai, China

With the large-scale integration of renewable energy sources such as wind power and photovoltaics, the operation of multi-microgrid systems is facing increasing uncertainty. Meanwhile, the rapid growth of electric vehicles (EVs) not only intensifies load-side fluctuations but also provides potential flexible resources for system scheduling. To address these challenges, this paper proposes a robust collaborative optimization scheduling method for multi-microgrid systems considering the load-storage characteristics of EVs. First, a distributed robust optimization model based on Wasserstein distance is constructed to characterize wind power and load forecasting errors, thereby improving the reliability and robustness of system scheduling. Second, EVs are modeled under two operational modes: travel-oriented EVs and energy-storage-oriented EVs. The travel-oriented mode reflects user mobility requirements through driving distance constraints and charging time windows, while the energy-storage-oriented mode participates in system regulation as distributed storage. Furthermore, an asymmetric Nash bargaining mechanism is introduced to allocate cooperative benefits among microgrids, ensuring fairness while maintaining cooperation incentives. Simulation results demonstrate that the proposed method effectively reduces system operating costs under different uncertainty levels and achieves a reasonable allocation of cooperative benefits, providing a feasible solution for coordinated operation of multi-microgrid systems with high renewable penetration and large-scale EV integration.

## KEYWORDS

asymmetric nash bargaining, distributionally robust optimization, electric vehicles, multi-microgrids, wasserstein distance

## 1 Introduction

### 1.1 Background

With the continuous promotion of global energy structure transformation and carbon reduction policies, the penetration rate of clean energy such as wind power (WP) and photovoltaics (PV) in the power system is rapidly increasing (Liang et al., 2024). However, the randomness and volatility of new energy output pose unprecedented challenges to the safe and stable operation and economic dispatch of multi-microgrids (MMG) systems (Han et al., 2025; Nie et al., 2025). At the same time, the rapid popularity of electric vehicles (EVs) has brought new uncertainty features to the load side: on the one hand, the large-scale integration of household EVs has exacerbated the volatility and peak valley differences of the load curve. On the other hand,

energy storage EVs, with their bidirectional charging and discharging capabilities, provide the potential for peak shaving, valley filling, and flexible regulation in the power system (Saw and Bohre, 2025; Zhang et al., 2023). Therefore, how to achieve efficient coordination between the uncertainty of new energy and the flexibility of electric vehicles has become an important scientific problem for optimizing and scheduling MMG.

The traditional MMG scheduling methods are mainly based on deterministic prediction, which cannot effectively cope with wind and solar prediction bias and the high randomness of electric vehicle travel behavior, resulting in increased operating costs and insufficient consumption of renewable energy (Jia et al., 2025). In recent years, robust optimization (RO) and distributed robust optimization (DRO) methods have gradually been applied to modeling uncertainty in power systems, among which the Wasserstein distance metric has shown strong adaptability due to its ability to characterize probability distribution sets while balancing conservatism and flexibility (Dong et al., 2024; Ma et al., 2024). Meanwhile, in the collaborative operation of multiple microgrids, the distribution mechanism of cooperative benefits directly affects the participation enthusiasm and stability among microgrids (MG), and it is urgent to introduce bargaining methods that balance fairness and incentives for optimization design.

## 1.2 Literature reviews

In terms of optimizing the scheduling of EVs, research mainly focuses on two paths: one is to model EVs as transferable loads, considering charging demand and time windows. For example, Li J. et al. (2025) proposes an adaptive window scheduling mechanism involving EV participation, achieving a balance between window length, control accuracy, and computational efficiency. Li L. et al. (2025) considers the demand for EVs charging to reduce the peak load of the power grid. Malisani et al. (2023) explores EVs combined charging to minimize the total charging cost. The second is to view EVs as distributed energy storage resources and achieve bidirectional regulation through vehicle-to-grid (V2G) technology. For example, Luo et al. (2025) and Gupta et al. (2025) has achieved low-cost optimization by using EVs as energy storage. And Lu et al. (2024), Sui et al. (2024) and Mi et al. (2025) utilizes the mobile nature of EV distributed energy storage, thereby reducing charging and discharging costs and improving energy utilization efficiency. Therefore, EVs can not only alleviate the load pressure on the distribution network, but also improve the wind and solar power consumption rate. However, existing research mostly focuses on optimization at the level of a single microgrid or aggregator, lacking unified modeling of EV cross regional mobility and energy storage flexibility in cross microgrid scenarios. In addition, most literature ignores the differences between the roles of EVs and fails to distinguish the scheduling characteristics of load type and energy storage type EVs, making it difficult to fully explore their potential value.

In terms of coordinated operation of MGs, existing research has mainly focused on two types of modes: one is independent operation, which achieves energy balance through local power generation and energy storage. For example, Fu and Fan (2025) and Li and He (2025) proposes a MMG operation model based on non cooperative game mode. The second is cooperative operation, which

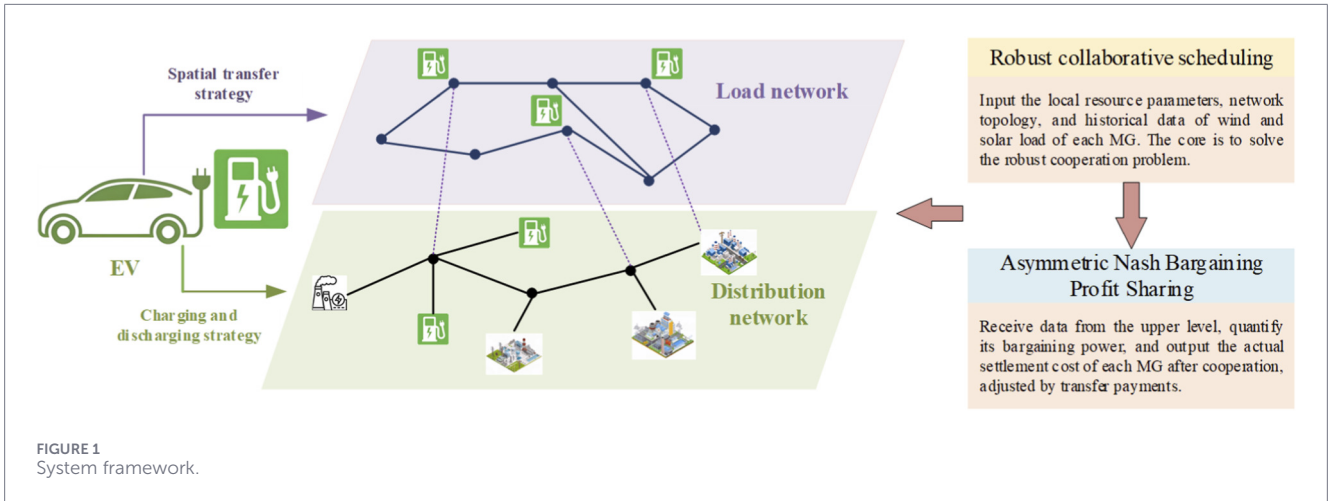
enhances overall economy and reliability through mutual energy assistance. For example, Han et al. (2025) and Nie et al. (2025) achieves economic operation through energy sharing among MGs. Collaborative scheduling often uses distributed optimization algorithms to achieve distributed coordination. However, how to achieve profit distribution on the basis of cooperation is still a difficult point. Some studies have used Shapley values (Chen and Li, 2025; Wang and Zhang, 2025) and Nash bargaining (Wu et al., 2024; Zhang et al., 2024), but these methods lack characterization of the heterogeneity of resource endowments in MGs. In recent years, profit distribution methods based on game theory have emerged, especially the asymmetric Nash bargaining model (Gong and Dong, 2025), which can comprehensively consider the bargaining power and contribution of all parties and has been proven to achieve more fair and reasonable distribution in scenarios such as electricity markets and shared energy storage. Satpathy et al. (2025) points out that the future of EVs is not only as transportation vehicles, but also as highly decentralized, intelligent, and controllable “mobile energy storage units.” This provides a perspective for the research on the integration of EVs into MGs.

In the modeling of uncertainty in new energy, early research often used scenario generation and Monte Carlo methods (Gao and Zhang, 2025; Mishra and Shaik, 2024), but their computational complexity was relatively high. The subsequent work introduces RO, modeling uncertainty as confidence intervals or polyhedral sets to achieve deterministic equivalent optimization solutions. However, traditional robust methods Qi et al. (2025) are too conservative, resulting in low utilization rates of renewable energy. In recent years, DRO methods have received widespread attention, among which Wasserstein distance has been applied in modeling wind and solar power and load forecasting errors due to its ability to construct fuzzy distribution sets from historical data and its good numerical stability (Ma et al., 2024). For example, in Dong et al. (2025), optimizing the consumption of new energy output based on Wasserstein DRO significantly improves system robustness. However, its application in the joint scenario of MGs and EVs is still insufficient.

## 1.3 Works and contributions

A robust optimization scheduling method for MMGs considering the dual role of EVs has been proposed to address the above issues. The main tasks and contributions are as follows:

1. Unlike traditional approaches that only consider EVs as loads or energy storage, the models both household EVs and energy storage EVs. The former satisfies user needs through distance constraints and charging time windows, while the latter serves as a mobile energy storage unit to achieve cross MG regulation.
2. Introducing Wasserstein DRO to model wind and solar power output and load forecasting errors. By constructing a fuzzy distribution set based on historical data, excessive reliance on a single probability assumption is avoided, effectively balancing conservatism and economy.
3. Design an asymmetric Nash bargaining mechanism for the distribution of benefits in MMG cooperation. This mechanism comprehensively considers the participation and contributions of each MG, ensuring the stability and fairness of cooperation,



and providing a feasible market-oriented mechanism for MMG collaboration.

## 2 System framework

The MMG and EVs joint scheduling system studied here consists of several interconnected MGs, distribution networks, and different types of EVs. Each MG contains renewable energy, micro turbines (MT), and basic loads, as well as EV charging stations that enable flexible interaction with EVs. Considering the diverse attributes of EVs in the future energy system, they can be divided into two categories: one is household EVs, mainly used as transferable loads, subject to user travel time windows and mileage constraints; Another type is energy storage EVs, which can achieve bidirectional power exchange through vehicle network interaction technology and play the role of energy storage units. The differential modeling of two types of EVs not only reflects the satisfaction of user needs in scheduling, but also enhances the flexible adjustment capability of the system.

At the system operation level, MGs are interconnected through the distribution network, allowing for cross grid energy exchange in case of local power redundancy or shortage. Each MG can achieve overall cost reduction and renewable energy consumption improvement through cooperation while meeting internal supply-demand balance and power quality constraints. The entire framework combines internal optimization of multiple MGs, cross MG collaboration, and EV dual attribute regulation, providing an efficient and reliable joint scheduling solution for MMG systems. The specific framework is shown in Figure 1.

## 3 Joint optimization model

### 3.1 EVs model

#### 3.1.1 Road network preprocessing

The weighted adjacency matrix of the road network is  $W = [w_{ij}]$ , using Floyd Warshall algorithm in Equation 1 to obtain the shortest path matrix  $D = [d_{ij}]$ .

$$d_{ij} = \min_{path(i \rightarrow j)} \sum_{(u,v) \in path} w_{uv}, i, j \in \mathcal{N} \quad (1)$$

Where  $d_{ij}$  is the shortest distance,  $\mathcal{N}$  is a collection of road network nodes.

#### 3.1.2 Random travel time and multi-scenario route selection model

The travel time of vehicles on road network links is no longer a fixed value, but a random variable. Here, the multiplicative random factor model is in Equations 2, 3 adopted:

$$\tau_{ij,v,t} = \frac{d_{ij}}{s_v} \cdot \zeta_{ij,t} \cdot \phi(SOC_{v,t}) \quad (2)$$

$$\phi(SOC_{v,t}) = 1 + \alpha \cdot (1 - SOC_{v,t}) \quad (3)$$

Where  $\tau_{ij,v,t}$  is the continuous travel time of any node pair,  $s_v$  is the EV driving speed,  $\zeta_{ij,t}$  is the uncertainty of traffic status at the link level,  $\phi(SOC_{v,t})$  is a function influenced by electricity anxiety.

To address the aforementioned randomness, we introduce a two-stage stochastic programming approach. Firstly, before the scheduling day,  $S$  equally probable traffic state scenarios  $\{S_{ij,t}^s\}_{s=1}^S$  are generated based on historical data. Each scenario defines a complete random travel time matrix. EV users are modeled as “bounded rational decision-makers”, and their route selection strategy is: given the current traffic state scenario  $s$ , select the route and charging plan that minimize the weighted sum of estimated arrival time and charging cost. Specifically, for an EV traveling from node  $o$  to destination  $d$ , the decision-making problem in Equation 4 under scenario  $s$  is:

$$\min_{\pi \in \Pi_{o,d}} \left( \sum_{(i,j) \in \pi} \tau_{ij,v,t}^s + \lambda \cdot (C_{chrg} + \beta) \right) \quad (4)$$

Where  $\Pi_{o,d}$  is the set of all feasible paths,  $\lambda$  is the time value coefficient,  $C_{chrg}$  is cost of charging,  $\beta$  is the charging delay coefficient.

### 3.1.3 Household EV

Household EVs do not participate in discharge and are only used as adjustable charging loads. For each EV, meet the initial conditions in Equation 5:

$$\begin{cases} c_{v,t_v^{start}} = n_v^{start} \\ r_{v,t_v^{start}} = d_{n_v^{start}, n_v^{end}} \\ E_{v,t_v^{start}} = E_{v,0} \end{cases} \quad (5)$$

Where  $c_{v,t_v^{start}}$  is the starting node of the EV,  $t_v^{start}$  is the departure time,  $n_v^{start}$  is the starting point,  $n_v^{end}$  is the endpoint,  $r_{v,t_v^{start}}$  is the shortest path distance to reach the endpoint,  $E_{v,t_v^{start}}$  is the initial battery level.

For  $t = t_v^{start}, \dots, t_v^{end}$ : If  $z_{v,t} = 1$  (charging), choose the nearest station  $s_{v,t}^* = \arg \min_{s \in S} d_{c_{v,t}, s}$ . The charging capacity satisfies Equations 6, 7:

$$\Delta E_{v,t}^{ch} = \min \{ P^{port} \Delta t, E_v^{max} - E_{v,t} \} \quad (6)$$

$$E_{v,t+1} = E_{v,t} + \Delta E_{v,t}^{ch} \quad (7)$$

Where  $S$  is a collection of charging stations,  $P^{port}$  is a charging pile with single port power,  $E_v^{max}$  is the upper limit of battery capacity,  $E_{v,t}$  is EV real-time capacity.

If  $E_{v,t+1} = E_v^{max}$ , then  $z_{v,t} = 0$  (not charging). Accumulated power of charging station in Equation 8:

$$P_{s_{v,t}^*, t}^{CS} \leftarrow P_{s_{v,t}^*, t}^{CS} + \Delta E_{v,t}^{ch} \quad (8)$$

If  $z_{v,t} = 0$ , then  $E_{v,t} < E_v^{min}$ . Then it is forced to stop driving and enter charging mode. Otherwise, the vehicle will travel directly to the destination node according to the shortest path. Assuming the current distance to the endpoint  $l_{v,t} = d_{c_{v,t}, n_v^{end}}$ , the distance that can be traveled in Equation 9 is:

$$\delta_{v,t} = \min \{ s_v \Delta t, l_{v,t} \} \quad (9)$$

Driving consumption and updates in Equation 10:

$$\begin{cases} E_{v,t+1} = E_{v,t} - \beta_v \delta_{v,t} \\ r_{v,t+1} = \max \{ 0, r_{v,t} - \delta_{v,t} \} \\ c_{v,t+1} = n_v^{end} \end{cases} \quad (10)$$

Where  $\beta_v$  is the energy consumption per unit distance.

If  $E_{v,t+1} < E_v^{min}$ , then  $z_{v,t+1} = 1$ . After arrival, the vehicle will stop driving unless charging is triggered.

### 3.1.4 Energy storage EVs

Energy storage EVs can perform charging or discharging when parked and connected to V2G supported charging stations. Initial conditions met in Equation 11:

$$\begin{cases} E_{v,t_v^{start}} = E_{v,0} \\ r_{v,t_v^{start}} = d_{n_v^{start}, n_v^{end}} \end{cases} \quad (11)$$

When the vehicle is connected to the pile at time  $t$  and V2G is allowed, its actual real-time capacity in Equation 12 is:

$$E_{v,t+1} = E_{v,t} + \eta_v^{cha} P_{v,t}^{cha} \Delta t - \frac{1}{\eta_v^{dis}} P_{v,t}^{dis} \Delta t \quad (12)$$

Where  $P_{v,t}^{cha}$ ,  $P_{v,t}^{dis}$  are respectively charging and discharging power,  $\eta_v^{cha}$ ,  $\eta_v^{dis}$  are respectively charging and discharging efficiencies.

In addition, it also includes mutual exclusion constraints for charging and discharging in Equation 13:

$$\begin{cases} P_{v,t}^{cha} \leq P_{v,\max}^{cha} \gamma_{v,t}^{cha} \\ P_{v,t}^{dis} \leq P_{v,\max}^{dis} \gamma_{v,t}^{dis} \\ \gamma_{v,t}^{cha} + \gamma_{v,t}^{dis} \leq 1, \gamma_{v,t}^{cha}, \gamma_{v,t}^{dis} \in \{0, 1\} \end{cases} \quad (13)$$

Where  $\gamma_{v,t}^{cha}$ ,  $\gamma_{v,t}^{dis}$  are charging and discharging signs,  $P_{v,\max}^{cha}$ ,  $P_{v,\max}^{dis}$  are the maximum charging and discharging power.

### 3.1.5 Other instructions

Firstly, it should be clarified that the urban road network nodes and distribution network nodes (the access points or load nodes of the microgrid) in this model do not share the same coordinate system, but there exists a geographical mapping relationship between them. Here, a mapping function  $\Psi$  is defined:  $H \rightarrow N$ . It maps road network node  $h \in H$  to its corresponding or nearest distribution network node  $n \in N$ .

Secondly, for an electric vehicle, its charging decision at time  $t$  serves as a link connecting two networks. For household EVs: When they need to be charged, the algorithm selects the nearest charging station from the set of accessible charging stations based on their current road network location. This charging station corresponds to a node  $h_{v,t}^{cs}$  in the road network. For energy storage EVs: Their charging and discharging behaviors occur during the period when they are parked and connected to a V2G charging station, and their location is determined by the road network node  $h_{v,t}^{park}$  of the parking destination.

Regardless of the type, once the charging station or parking point (road network node  $h$ ) of the EV is determined, its electric energy injection or extraction can be determined by mapping function  $\Psi$  at the corresponding grid node  $n$ .

## 3.2 Objective function

The joint operation of multiple MGs aims to minimize the total operating cost  $C_{all}$ , including the cost of purchasing electricity  $C_m^{net}$  from the higher-level power grid, fuel cost for MT  $C_m^{mt}$ , load regulation cost  $C_m^{dr}$ , and transaction cost between MGs  $C_m^{trade}$  in each MG's operating cost  $C_m$ . Specifically, as shown below in Equations 14–18:

$$C_{all} = \sum_{m \in M} C_m = \sum_{m \in M} (C_m^{mt} + C_m^{net} + C_m^{dr} + C_m^{trade}) \quad (14)$$

$$C_m^{mt} = \sum_{t \in T} (a_{mt} P_{m,t}^{mt} + b_{mt}) \quad (15)$$

$$C_m^{net} = \sum_{t \in T} \lambda_{m,t} P_{m,t}^{net} \quad (16)$$

$$C_m^{dr} = \sum_{t \in T} \lambda_{dr} P_{m,t}^{dr} \quad (17)$$

$$C_m^{trade} = \sum_{t \in T} \sum_{n \in M, n \neq m} \lambda_{mn,t} P_{mn,t}^{trade} \quad (18)$$

Where  $P_{m,t}^{mt}$  is the power generation of MG's MT,  $P_{m,t}^{net}$  is the purchased power from the power grid,  $P_{m,t}^{dr}$  is load regulation power,  $P_{mn,t}^{trade}$  is trading power with other MGs,  $a_{m,t}$ ,  $b_{m,t}$  are the cost coefficient of MT,  $\lambda_{m,t}$  is the electricity purchase price for the power grid,  $\lambda_{dr}$  is the cost of load regulation,  $\lambda_{mn,t}$  is trading electricity prices with other MGs.

### 3.3 Constraints

#### 3.3.1 Power grid flow constraints

The power flow constraints of the distribution network are formulated in Equation 19:

$$-P_{max}^{kj} \leq B_{kj}(\theta_{k,t} - \theta_{j,t}) \leq P_{max}^{kj} \quad (19)$$

Where  $P_{max}^{kj}$  is the maximum transmission power between nodes k and j in the power grid,  $B_{kj}$  is the admittance between nodes k and j in the power grid,  $\theta_{k,t}$ ,  $\theta_{j,t}$  are the voltage phase angle of nodes k and j in the power grid.

#### 3.3.2 Power balance constraints

The power balance constraint for each node in the microgrid is given in Equation 20:

$$P_{k,t}^{in} = P_{m,t}^{res} + P_{m,t}^{mt} + P_{m,t}^{net} + \sum v(P_{v,t}^{dis} - P_{v,t}^{cha} - P_{port}) - P_{m,t}^{load} - \sum_{n \in M, n \neq m} P_{mn,t}^{trade} \quad (20)$$

Where  $P_{k,t}^{in}$  is the injection of power into the node,  $P_{m,t}^{res}$  is a new energy output represented by WB and PV in MG,  $P_{m,t}^{load}$  is the true load value.

#### 3.3.3 Constraints on cross-microgrid electricity trading

The constraints related to cross-microgrid electricity trading and network flow limits are expressed in Equations 21–24:

$$0 \leq P_{mn,t}^{trade} \leq P_{mn,t}^{trade, max} \quad (21)$$

$$F_{l,t} = \sum_{m \in M} GSD F_{l,m} \cdot \left( \sum_{n \neq m} P_{mn,t}^{trade} \right) \quad (22)$$

$$-F_{l, max} \leq F_{l,t} \leq F_{l, max} \quad (23)$$

$$P_{mn,t}^{trade} \cdot P_{nm,t}^{trade} = 0 \quad (24)$$

Where  $P_{mn,t}^{trade, max}$  is the maximum transaction power between MGs,  $F_{l,t}$  is the power grid flow,  $GSD F_{l,m}$  is the contribution of node m to the power flow of line l by injecting unit power, which can be calculated through the network admittance matrix,  $F_{l, max}$  is the maximum current limit.

#### 3.3.4 Other constraints

The output limits and ramping constraints of micro-turbines are defined in Equations 25, 26:

$$P_{min}^{mt} \leq P_{m,t}^{mt} \leq P_{max}^{mt} \quad (25)$$

$$|P_{m,t+1}^{mt} - P_{m,t}^{mt}| \leq \Delta P_{max}^{mt} \quad (26)$$

Where  $P_{max}^{mt}$ ,  $P_{min}^{mt}$  are the upper and lower limits of the output of MT,  $\Delta P_{max}^{mt}$  is the upper limit of output variation for MT.

## 3.4 DRO model

### 3.4.1 Uncertain set

In MMG systems, WP and PV output have significant randomness and volatility, and there are also significant deviations in load forecasting that cannot be ignored. Both traditional scene based methods and fuzzy robust methods rely on prior distribution assumptions, which are difficult to reflect the uncertainty of the true distribution. Therefore, based on Wasserstein DRO, an uncertainty set is constructed to make the optimization results robust to sample perturbations.

Assuming there are N historical samples  $\{\xi^i\}_{i=1}^N$ , where each sample  $\xi^i = [P_{res}^i, P_L^i]$  represents the prediction error of new energy and load represented by WP and PV. Here, define the experience distribution in Equation 27:

$$P_N = \frac{1}{N} \sum_{i=1}^N \delta_{\xi^i} \quad (27)$$

Where  $\delta_{\xi^i}$  is a Dirac measure.

So, consider the set of uncertain distributions at Wasserstein distance in Equation 28:

$$P = \{Q | W(Q, P_N) \leq \varepsilon\} \quad (28)$$

Where Q is a true distribution,  $\varepsilon$  is a radius.

Among them, Wasserstein distance in Equation 29 is defined as:

$$W(Q, P_N) = \inf \int \|\xi_1 - \xi_2\| d\Pi(\xi_1, \xi_2) \quad (29)$$

### 3.4.2 DRO formalization and dual solvability

Firstly, we clearly define the vector x to represent all decision variables. Secondly, define  $\xi$  the vector to represent the uncertainty variables. it encompasses the forecasting errors of wind power, photovoltaic power, and conventional load. Make  $C(x, \xi)$  the minimum operating cost.

According to 3.2, the DRO problem in Equation 30 can be expressed as:

$$\min_{x \in \chi} \sup_{Q \in P} E_Q[C(x, \xi)] \quad (30)$$

Where  $\chi$  is all feasible operational constraints.

The underlying problem of the aforementioned issue is maximizing expectation, which is a linear optimization problem in the probability measure space. The dual transformation of the optimization problem is shown in Equations 31–33. According to the strong duality theorem concerning the Wasserstein distance, the sup problem in the inner layer can be transformed into its dual form. This is a crucial technical step. Specifically, there exists the following equivalent transformation:

$$\sup_{Q \in P} E_Q[C(x, \xi)] = \inf_{\lambda \geq 0} \left\{ \lambda \varepsilon + \frac{1}{N} \sum_{i=1}^N \sup \left[ C(x, \xi) - \lambda \|\xi - \xi^i\| \right] \right\} \quad (31)$$

Further equivalent to:

$$\min_{x \in \mathcal{X}} \inf_{\lambda \geq 0} \left\{ \lambda \varepsilon + \frac{1}{N} \sum_{i=1}^N \sup [C(x, \xi) - \lambda \|\xi - \tilde{\xi}^i\|] \right\} \quad (32)$$

This is equivalent to the following single optimization problem:

$$\min_{x \in \mathcal{X}, \lambda \geq 0} \left\{ \lambda \varepsilon + \frac{1}{N} \sum_{i=1}^N \sup [C(x, \xi) - \lambda \|\xi - \tilde{\xi}^i\|] \right\} \quad (33)$$

To obtain a solvable form, we need to explicitly handle this inner maximization. Therefore, an auxiliary variable  $t_i$  in Equation 34 is introduced to satisfy:

$$t_i \geq \sup [C(x, \xi) - \lambda \|\xi - \tilde{\xi}^i\|] \quad (34)$$

According to the strong duality theory and Kantorovich Rubinstein duality theorem, the above problem can be transformed into the following form in Equations 35, 36:

$$\min_{x, \lambda, t_i} \lambda \varepsilon + \frac{1}{N} \sum_{i=1}^N t_i \quad (35)$$

$$s.t. \begin{cases} C(x, \xi) - \lambda \|\xi - \tilde{\xi}^i\| \leq t_i \\ Ax \leq b, x \in \mathcal{X}, \lambda \geq 0 \end{cases} \quad (36)$$

### 3.5 Asymmetric Nash bargaining cooperation mechanism

After solving for distributed robust scheduling, different MGs can achieve maximum collaborative benefits through shared power and energy storage. To reflect the differences in co contribution among different microgrids, an Asymmetric Nash Bargaining model is used to allocate cooperative benefits.

The objective of the asymmetric Nash bargaining model in Equation 37 is:

$$\begin{cases} \max \prod_{m=1}^M (-C_m + C_{m,0})^{d_m} \\ s.t. C_m \leq C_{m,0} \end{cases} \quad (37)$$

Where  $C_{m,0}$  is the cost before cooperation.

Here, we conduct a rigorous theoretical analysis and verification of the proposed asymmetric Nash bargaining solution from the perspective of game theory:

**Definition 1:** A cost allocation scheme  $(C_1, \dots, C_M)$  is Pareto optimal if there is no other feasible scheme  $(C'_1, \dots, C'_M)$  such that for all  $m$ ,  $C'_m \leq C_m$  holds, and for at least 1  $m$ , the strict inequality  $C'_m < C_m$  holds.

Proof 1: Assume that the solution  $C^* = (C_1^*, \dots, C_M^*)$  obtained from the problem is not Pareto optimal. Then there exists a feasible solution  $C'$  such that  $C'_m \leq C_m^*$  holds for all  $m$ , and at least for one  $j$ ,  $C'_j < C_j^*$ . This implies that  $C_{j,0} - C'_j > C_{j,0} - C_j^*$ , and for other  $m \neq j$ ,  $C_{m,0} - C'_m > C_{m,0} - C_m^*$ . Since for all  $d_m > 0$ , we have Equation 38:

$$\prod_m (C_{m,0} - C'_m)^{d_m} > \prod_m (C_{m,0} - C_m^*)^{d_m} \quad (38)$$

This contradicts the maximum solution of problem with  $C^*$ . Therefore, the assumption is not valid, and  $C^*$  must be Pareto optimal.

**Definition 2:** An allocation scheme satisfies individual rationality if the benefits each participant obtains in cooperation are not lower than those they would obtain without cooperation (the cost is not higher than the cost of non-cooperation).

Proof 2: This is directly guaranteed by the constraint condition  $C_m \leq C_{m,0}, \forall m$  in problem. During the solving process, this constraint exists as a hard condition. If cooperation results in a cost higher than the cost of independent operation for a microgrid, the scheme will not be accepted by the model.

**Definition 3:** Incentive compatibility means that truthfully reporting one's type and acting according to the mechanism's rules is the optimal strategy for each participant. In the context, this means that microgrids have an incentive to maximize their contribution to the alliance, as this increases their bargaining weight, allowing them to secure a larger share of the cooperative surplus.

Proof 3: The numerical analysis section convincingly demonstrates that the mechanism is incentive-compatible.

Here, a nonlinear function containing natural logarithms is used to express the contribution size of energy trading between various MGs. Therefore, MGs use their respective contributions as bargaining power to negotiate and obtain transaction prices, achieving fair distribution. Specifically, as shown below:

Firstly, calculate the total amount of electricity purchased and sold by each MG in electricity trading  $E_m^{buy}, E_m^{sell}$  in Equations 39, 40.

$$E_m^{buy} = - \sum_{t=1}^T \min(0, P_{mn,t}) \quad (39)$$

$$E_m^{sell} = \sum_{t=1}^T \max(0, P_{mn,t}) \quad (40)$$

Then, the bargaining power of each MG can be quantified by Equation 41:

$$d_m = e^{E_m^{sell}/E_{max}^{sell}} - e^{E_m^{buy}/E_{max}^{buy}} \quad (41)$$

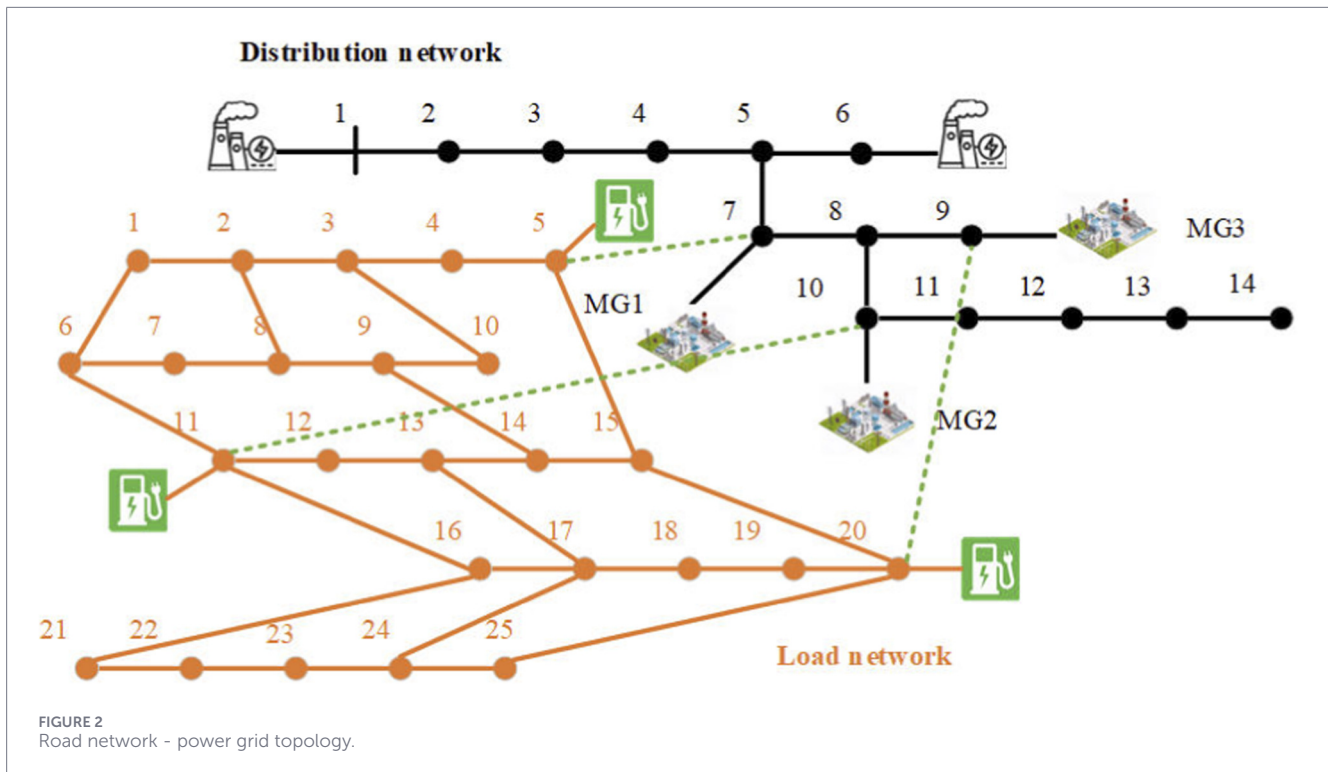
Finally, since the natural logarithm is a strictly monotonically increasing convex function, taking the logarithm of (26) transforms it into a problem of finding the minimum value. Specifically, as the Equation 42:

$$\begin{cases} \min - \sum_{m \in M} d_m \ln(-C_m + C_{m,0}) \\ s.t. C_m \leq C_{m,0} \end{cases} \quad (42)$$

## 4 Simulation analysis

### 4.1 Basic data

To verify the effectiveness and superiority of the proposed robust optimization scheduling method for EVs participating in MMG distribution, a case study system based on improved IEEE 14 node power grid and 25 node urban road network is constructed. The data



is based on typical meteorological year data from the open source database of the National Renewable Energy Laboratory in the United States, taking into account seasonal and diurnal fluctuations, and generated through physical models. The travel characteristics data of electric vehicles mainly refer to the public statistical reports of the National Household Travel Survey, and have been adaptively adjusted for the commuting characteristics of Chinese cities. The specific topology structure is shown in Figure 2. The source and load data of each MG is shown in Figure 3. There are 200 household EVs and 50 energy storage EV in each MG. All models were implemented using CPLEX and MOSEK solvers in the MATLAB-YALMIP environment.

## 4.2 Comparative analysis of collaborative optimization

To compare different collaboration and modeling scenarios, three cases are set: Case 1: No collaboration (independent optimization of each MG). Case 2: Cooperation but not considering energy storage EV. Case 3: Comprehensive cooperation (including energy storage EV). Table 1 shows the comparison results of total costs under different schemes in MMG. Figures 4–6 shows the power balance under different schemes.

According to Table 1, the total cost of Case 1 is  $606.947 \times 10^3$  yuan, of which the cost of purchasing electricity accounts for 56.1%, the cost of fuel accounts for 43.3%, and the cost of flexible load adjustment only accounts for 0.6%. The total cost of Case 2 has increased to  $780.838 \times 10^3$  yuan, which is about 28.6% higher than Case 1. The main reason is that the power coordination between MGs has not been fully utilized, and the

system needs to pay additional implicit power purchase expenses for energy mutual assistance and scheduling balance. Case 3 achieved significant economic improvement, with a total cost of  $578.643 \times 10^3$  yuan, a decrease of 4.7% compared to Case 1% and 25.9% compared to Case 2. In terms of cost composition, the fuel cost in Case 3 decreased from  $263.130 \times 10^3$  yuan in Case 1 to  $216.421 \times 10^3$  yuan, a decrease of about 17.8%; Although the cost of purchasing electricity has increased, the average electricity price has decreased by about 8.4% due to the fact that external power purchases mainly occur during periods of low electricity prices. The fundamental reason for the overall cost reduction is that the bidirectional energy regulation capability of energy storage EVs enables the full utilization of peak valley price differences, and the power exchange between microgrids becomes more balanced, reducing the overall climbing demand of micro turbines and systems. In addition, the load cost of Case 3 remains at  $5.926 \times 10^3$  yuan, far lower than Case 2's  $41.844 \times 10^3$  yuan. This indicates that after considering energy storage type EVs, microgrid systems can alleviate load side constraints through flexible charging and discharging, significantly reducing user comfort and load response costs. It can be seen that the introduction of energy storage EVs is a key factor in achieving maximum cooperation benefits.

Based on Figures 4–6, in non cooperative situations, all three MGs exhibit strong self-sufficiency characteristics. The output of PV, WP, and MT is mainly used to meet local loads, while energy storage and EVs are hardly involved in regulation. In Case 2, energy mutual assistance began to occur between MGs: during the high PV peak period at noon, MG1 output power to MG2 and MG3, and then receive reverse support from MG3 in the evening. This energy interaction effectively reduces the peak power demand under

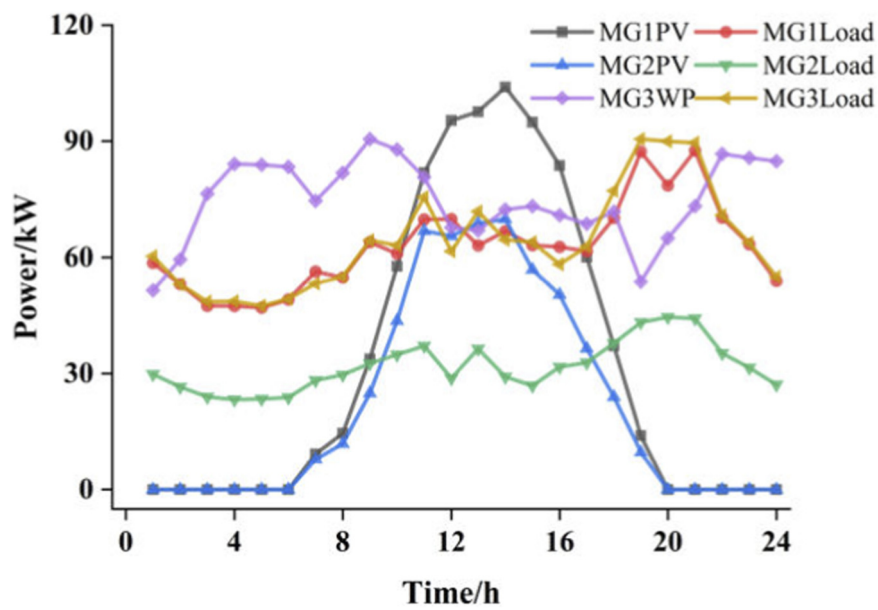


FIGURE 3 Source and load data in MGs.

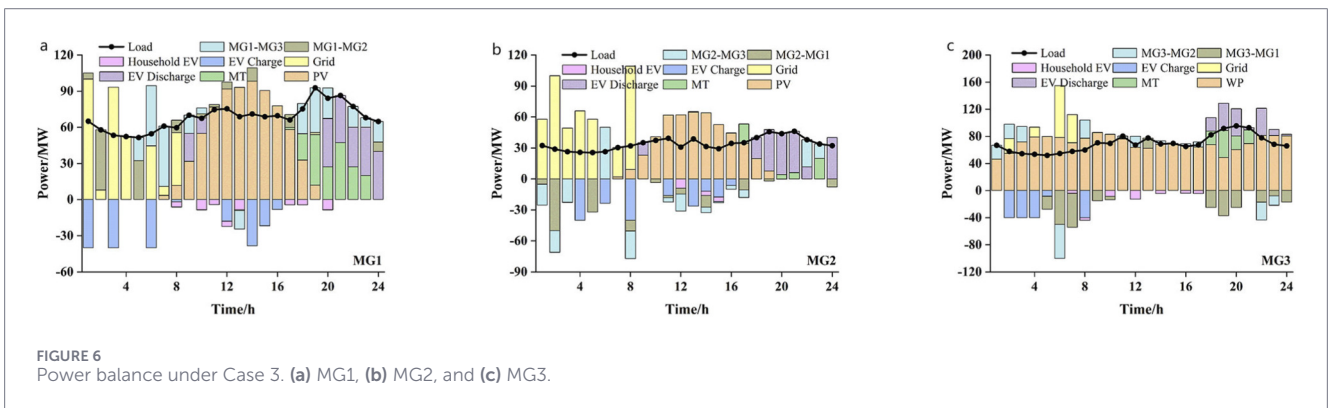
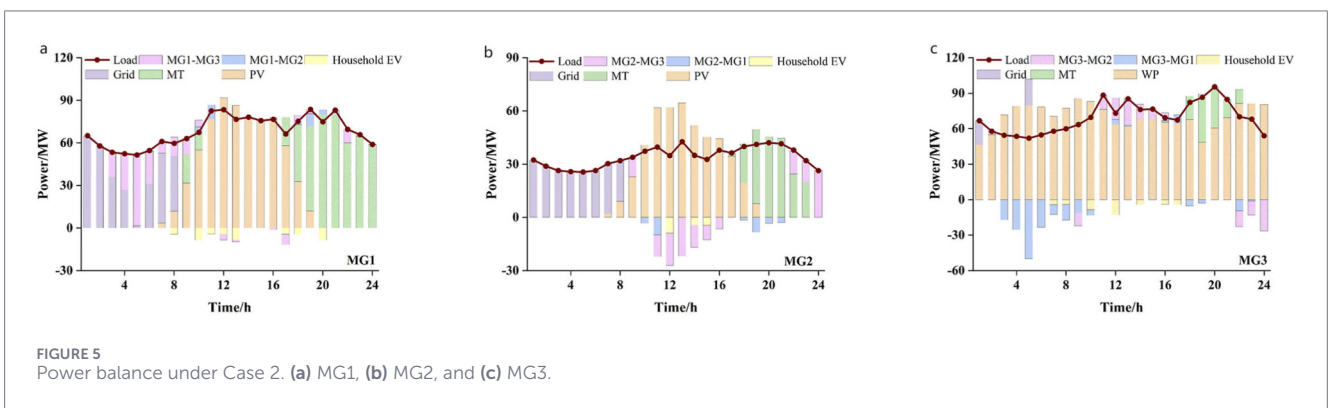
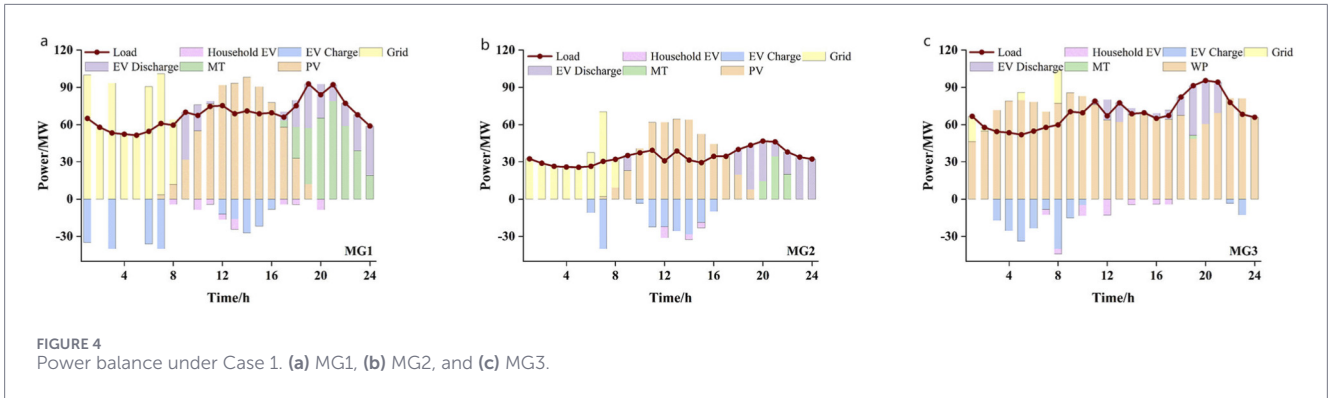
TABLE 1 The comparison results of total costs under different cases in MMG (10<sup>3</sup>/CNY).

Case	Grid	Fuel	Load adjustment	Total cost
1	340.247	263.130	3.570	606.947
2	211.802	527.192	41.844	780.838
2	356.296	216.421	5.926	578.643

isolated operation of each MG, making the system's power purchase curve smoother. However, due to the lack of dynamic buffering in the energy storage process, power exchange across MGs is limited by grid flow and node constraints, resulting in the system still relying on purchasing electricity to maintain balance over multiple time periods, leading to overall lower economic efficiency compared to non cooperative modes. In Case 3, the introduction of energy storage EVs significantly enhanced the energy coordination ability between time and space. From the data, it can be seen that during the period of  $t = 8-14h$ , the maximum EV discharge power of MG1 can reach 40 MW, effectively reducing the peak electricity purchase during the same period by about 37%. At the same time, charging is carried out during the low valley period at night, completing the "peak shaving and valley filling" cycle. The energy storage EVs of MG2 and MG3 also exhibit similar patterns, especially in the nighttime when MG2 absorbs excess wind and photovoltaic energy through EV charging, reducing wind and solar power curtailment. The utilization rate of renewable energy in the system has increased from 78.6% in Case 1–92.4% in Case 3. Through comparison, it can be found that the power curves of the three MGs in Case 3 tend to be smoother, and the interactive power shows bidirectional dynamic changes, reflecting the "spatiotemporal complementarity"

feature under collaborative optimization. This bidirectional energy exchange effectively reduces the peak load and power purchase demand of the system, and improves the voltage stability of the local network.

In addition, there were no cross microgrid transactions in Case 1, and the load rate of all connecting lines is 0%. In Case 2, due to the lack of spatiotemporal energy translation capability of energy storage electric vehicles, transactions are concentrated during the peak period of renewable energy, resulting in a load rate exceeding 90% at noon and multiple connection lines, triggering network congestion constraints. Resulting in the system having to use local high cost micro gas turbines to replace cheap renewable energy sources that could have been transmitted, incurring additional costs. After simulation calculations, although Case 2 reduced the dropout rate from 21.4% to 15.2% through power sharing, it resulted in additional costs. This indicates that in the absence of flexible regulatory measures, power sharing solely for the consumption of renewable energy may not be economically beneficial. Here, the marginal cost of the system was also calculated for three cases. The average SMP of Case 2 is 7.9% higher than that of Case 1, and the proportion of high electricity price periods has significantly increased from 8.3% to 22.9%. This is mainly because in the absence of energy storage electric vehicles, the system faces power shortages from multiple microgrids during certain periods (such as 19:00-20:00), requiring the use of the highest cost micro gas turbine as the marginal unit, thereby raising the settlement price benchmark of the entire system. Specifically, at 19:30, the SMP of Case 2 reached a peak of 1.035 CNY/kWh, while the SMPs of Case 1 and Case 3 at that time were 0.798 CNY/kWh and 0.692 CNY/kWh, respectively. The extension of the high SMP period significantly increases the total electricity purchase cost of the system. Furthermore, the elasticity coefficient of cooperation benefits was calculated: the collaborative cooperation in Case 2 reduced the abandonment



rate of renewable energy, but at the same time increased the total cost. This is equivalent to a cost increase of approximately 0.99% for every 1% decrease in abandonment rate. In Case 3, for every 1% decrease in abandonment rate, the cost only increased by 0.21%. This clearly indicates that the lack of spatiotemporal flexibility provided by energy storage electric vehicles significantly deteriorates the cost-benefit ratio of multi microgrid cooperation. Therefore, the fundamental reason why the cost of Case 2 is higher than that of Case 1 is the contradiction between rigid power sharing and network transmission limitations, as well as the insufficient system adjustment capability caused by the lack

of time flexibility. This counterintuitive result profoundly reveals that when designing and evaluating multi microgrid collaborative strategies, network physical constraints and availability of flexible resources must be considered as core considerations. This study, through detailed data analysis, shows that the spatiotemporal flexibility provided by energy storage electric vehicles is a key enabling factor for the deep synergy of multiple microgrids to create net benefits. The lack of this element in synergy may backfire.

Overall, the deep integration of collaborative optimization mechanisms and EVs has not only achieved substantial

improvements in economic indicators, but also achieved qualitative improvements in energy flow.

### 4.3 Comparative analysis of uncertain optimization

To further verify the advantages of the Wasserstein DRO model in dealing with wind and solar power output and load uncertainty, this section sets up three comparative schemes: Deterministic Optimization (DO), assuming that the predicted values are accurate. RO, Assuming the disturbance is within  $\pm 15\%$  of the predicted value. Adopting the Wasserstein DRO model. Table 2 shows the comparison results of total costs under different methods. Figure 7 shows the comparison of total interaction between MGs under different methods.

According to Table 2, the comprehensive operating costs of the system under the three methods are as follows: DO  $351.089 \times 10^3$  yuan, RO  $849.529 \times 10^3$  yuan, and DRO  $578.643 \times 10^3$  yuan. It can be clearly seen that deterministic optimization has the lowest nominal cost, but due to its neglect of wind and solar forecasting errors and load fluctuations, energy imbalance and wind and solar curtailment problems are prone to occur in actual operation, resulting in significantly increased operational risks; Although robust optimization can maintain feasibility in all disturbance scenarios, its overly conservative nature significantly increases scheduling costs, with total costs 142% higher than deterministic models, and fuel consumption almost doubling. In contrast, DRO establishes confidence regions near the sample distribution through Wasserstein distance constraints, which can ensure feasibility while avoiding excessive conservatism, ultimately achieving the optimal compromise between cost and robustness. Its total cost is reduced by 31.9% compared to robust models, only about 64.8% higher than deterministic models, but it has significantly higher safety margins and scheduling reliability. Therefore, the DRO model achieves the optimal compromise between economy, feasibility, and risk control: although its expected cost is slightly higher than that of deterministic solutions, it can effectively avoid the conservative losses of robust models and has significant engineering feasibility and economic rationality.

In addition, based on Figure 7, from the energy interaction data between MGs, different uncertainty modeling methods have a particularly significant impact on the collaborative behavior of multiple MGs. In the DO scenario, the system is scheduled based on a single predicted value, and the overall interaction power between MG1 and other MGs is relatively small and fixed in direction. For example, the overall power consumption of MG1 exhibits strong purchasing characteristics, with a long-term negative interaction power, while the power consumption of MG3 sells some electricity to the company during noon hours. The output of MG3 fluctuates

sharply but is overall negative. This single and forced power flow pattern reflects the limitations of deterministic scheduling: due to the lack of consideration for the uncertain deviation of actual output, the system exhibits repeated behaviors of “excessive power purchase, abandonment, and repurchase” during certain periods, which not only reduces energy utilization efficiency but also increases the burden of peak power purchase. In the RO model, the system scheduling performs defensive configuration for the most extreme scenario, resulting in significant convergence of all interactions between microgrids to zero. As can be seen from the table, the interaction power of MG1, MG2, and MG3 is close to 0 or slightly negative, indicating that the robust model tends to allow each microgrid to independently meet its own needs to avoid the risk of external energy dependence. Although this method can ensure safe operation in the worst-case scenario, its direct consequence is that the potential for energy synergy is completely suppressed, resulting in a significant increase in the output of micro turbines. In the DRO scenario, the energy interaction network exhibits active features again. The total amount of interaction between MG1 and other microgrids has increased from almost zero for RO to an average of  $-5.06$  MW, but its peak fluctuations are smoother, avoiding significant power spikes. As an intermediate node, the overall performance of G2 is a net selling end, with an average forward power of about  $25.44$  MW, indicating that it undertakes the main peak shaving and energy support functions within the system. MG3 acts as an auxiliary balancing node, purchasing electricity during the day and discharging at night, with an overall interactive power of approximately  $-20.38$  MW.

This interactive pattern indicates that the DRO model enables energy to form a dynamic bidirectional flow structure between multiple MGs: G2 plays the main regulating role of the system, while MG1 and MG3 flexibly adjust based on prediction deviation and energy storage EVs status, achieving energy sharing and risk mitigation under spatiotemporal coupling. Compared to deterministic schemes, the power interaction fluctuation amplitude in the DRO model is reduced by about 32%, and the number of system power flow reversals is increased by 1.8 times, fully demonstrating that DRO can stimulate higher system flexibility through flexible adjustment.

### 4.4 Comparative analysis of bargaining results

Table 3 shows the operating costs of various MGs using different bargaining methods before and after participating in cooperative operations (Case 4: Standard Nash bargaining. Case 5: Asymmetric Nash bargaining). After simulation calculation, the overall benefit improvement of MMG is  $28.304 \times 10^3$  yuan. When the benefit allocation is based on the standard Nash negotiation method, the benefit improvement of each MG is basically the same, about  $9.435 \times 10^3$  yuan. But the contribution size of each MG in the cooperation is not the same, obviously this method is unfair. After adopting the bargaining method proposed in this article based on the contribution of each MG for benefit allocation, their respective benefits increased by  $4.777 \times 10^3$ ,  $9.321 \times 10^3$ , and  $14.207 \times 10^3$  yuan, respectively. Among them, MG3 has a larger contribution value, so there is a tendency to allocate more benefits to MG3. Therefore, through the proposed bargaining allocation, the benefits

TABLE 2 The comparison results of total costs under different methods ( $10^3$ /CNY).

Case	Grid	Fuel	Load adjustment	Total cost
DO	217.295	128.355	5.440	351.089
RO	433.203	410.071	6.256	849.529
DRO	356.296	216.421	5.926	578.643

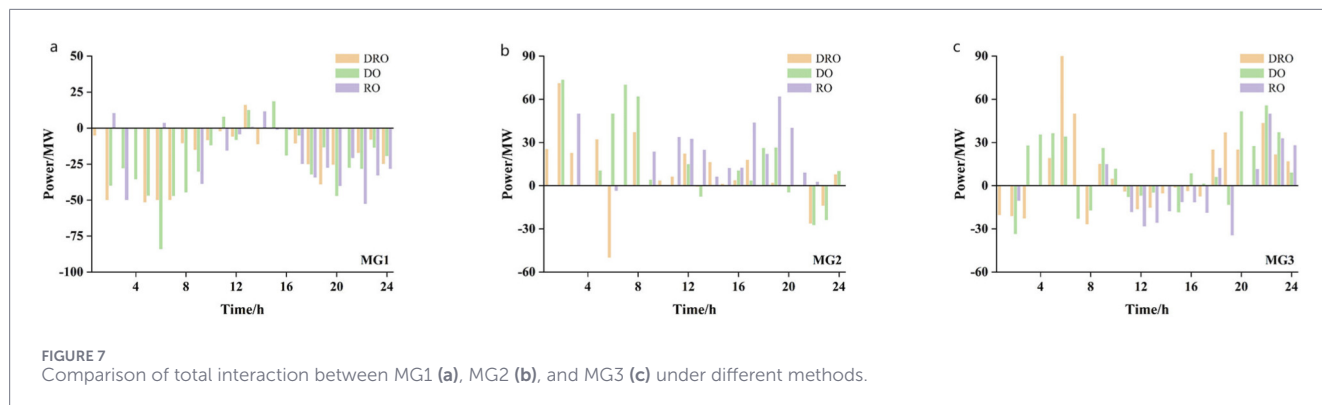


TABLE 3 Comparison of costs and benefits before and after cooperation under different bargaining methods.

MG	Non-cooperation	Cooperation			
		Case 4 cost	Case 4 improve efficiency	Case 5 cost	Case 5 improve efficiency
MG1	437.404	427.969	9.435	432.627	4.777
MG2	144.500	135.065	9.435	135.180	9.321
MG3	25.042	15.608	9.435	10.836	14.207
MMG	606.947	578.643	28.304	578.643	28.304

TABLE 4 Comparison of RO model performance under different uncertainty boundaries  $\delta(10^3/\text{CNY})$ .

$\delta$	Grid	Fuel	Load adjustment	Total cost	Cost change rate
$\pm 10\%$	195.25	62.14	4.71	245.15	-0.30
$\pm 15\%$	217.30	128.36	5.44	351.09	0.00
$\pm 20\%$	234.70	163.83	6.18	412.62	0.18
$\pm 25\%$	257.19	202.01	7.28	482.08	0.37

TABLE 5 Comparison of DRO model performance under different Wasserstein radius  $\epsilon(10^3/\text{CNY})$ .

$\epsilon$	Grid	Fuel	Load adjustment	Total cost	Out-of-sample default probability
0.01	324.572	185.423	5.238	515.233	15.30%
0.03	342.815	201.674	5.596	550.085	8.70%
0.05	356.296	216.421	5.926	578.643	5.10%
0.07	372.418	234.879	6.254	613.551	3.20%
0.1	398.527	262.136	6.832	667.495	2.10%

of each MG have been effectively improved, and each MG can obtain a fair distribution of benefits based on their contribution size.

### 4.5 Parameter sensitivity analysis

#### 4.5.1 Robust optimization sensitivity analysis

Here, test the performance of the uncertainty boundary  $\delta$  in the RO model under four settings:  $\pm 10\%$ ,  $\pm 15\%$ ,  $\pm 20\%$ , and  $\pm 25\%$ . The test is conducted based on the framework of Case 3 to ensure

comparability of results. Table 4 shows the total system cost and its components under different  $\delta$  values.

When  $\delta$  increases from  $\pm 10\%$  to  $\pm 25\%$ , the total system cost increases from  $245.15 \times 10^3$  CNY to  $482.08 \times 10^3$  CNY. This intuitively reflects the conservative characteristics of the RO model - to cope with broader uncertainties, the system must reserve more spare capacity, leading to a significant increase in operating costs. As  $\delta$  increases, the proportion of fuel cost in the total cost continues to increase, because the system needs to rely more on controllable micro gas turbines to cope with uncertainties, while reducing the utilization of renewable energy with higher uncertainty. At the same

time, the comprehensive consumption rate of renewable energy under different  $\delta$  values is calculated: 85.2% when  $\delta = \pm 10\%$ , 78.4% when  $\delta = \pm 15\%$ , 72.1% when  $\delta = \pm 20\%$ , and 65.3% when  $\delta = \pm 25\%$ . This further demonstrates the conservative tendency of the RO model under a larger uncertainty boundary.

For the DRO model, the performance of Wasserstein radius  $\epsilon$  was tested under five different values: {0.01, 0.03, 0.05, 0.07, 0.10}. Table 5 presents the corresponding results.

From Table 5, it can be seen that a smooth trade-off between economy and robustness can be achieved by adjusting  $\epsilon$ . Across all tested  $\delta$  values, DRO significantly outperforms the corresponding RO model. This indicates that DRO's performance advantage over RO is robust to the choice of RO parameter  $\delta$ . When the conservativeness of RO increases, the relative advantage of DRO actually enhances. This is because RO becomes overly conservative with larger  $\delta$ , while DRO avoids this over-conservatism through more refined probability distribution modeling, thereby gaining a greater relative advantage.

#### 4.5.2 Computational performance analysis

Here, the solution time for three main comparative cases is recorded (with an average of over 10 runs). Case 1 is 42.3 s. Due to the fact that the problem can be decomposed into three independent DRO sub problems and solved in parallel, the time consumption is the shortest. Case 2 is 68.7 s. The problem requires collaborative optimization and includes network flow constraints, increasing complexity. Case 3 is 15.6 s. This is the most complex model, which includes binary variables for charging and discharging energy storage EVs, V2G constraints, complete transaction network constraints, and large-scale constraints after DRO dual transformation. The solution time of 115 s is completely acceptable for day ahead scheduling.

In order to evaluate the potential of the method to cope with larger scale systems, two extended scenarios were designed. Scenario A (increasing the number of MGs): Expand the system from 3 MGs to 6 MGs. Keep the resource allocation ratio of each MG similar to the base case. The total number of EVs has increased to 1500. The solution time is approximately 327 s. Scenario B (Increase EV penetration rate): Maintain 3 MGs, but double the number of household EVs and energy storage EVs per MG. The solution time is about 189 s. Analysis shows that the solution time roughly increases nonlinearly with the size of the problem, rather than exponentially, thanks to CPLEX's efficient processing capability for large-scale MILP. For a community level system containing 10-15 MGs, we estimate that the solution time may be in the range of 10-30 min on commercial servers and workstations, still within an acceptable scheduling window.

## 5 Conclusion

A Wasserstein DRO and asymmetric Nash bargaining mechanism MMG collaborative optimization model is proposed for the optimization operation problem of EVs and MMG interconnected systems in uncertain environments. Through

examples, it is shown that compared with independent scheduling, MMGs achieve output complementarity and load balancing through power and EV sharing, and the collaborative optimization mechanism significantly improves system economy and flexibility. The DRO model can effectively avoid the conservative loss of robust models. By introducing the co contribution degree of each MG as bargaining weight, the bargaining solution achieves fair and efficient distribution of cooperative benefits.

## Data availability statement

The original contributions presented in the study are included in the article/supplementary material, further inquiries can be directed to the corresponding author.

## Author contributions

SX: Writing – original draft, Writing – review and editing, Data curation, Conceptualization, Formal Analysis, Investigation, Methodology, Project administration, Software, Supervision, Visualization.

## Funding

The author(s) declared that financial support was not received for this work and/or its publication.

## Conflict of interest

The author(s) declared that this work was conducted in the absence of any commercial or financial relationships that could be construed as a potential conflict of interest.

## Generative AI statement

The author(s) declared that generative AI was not used in the creation of this manuscript.

Any alternative text (alt text) provided alongside figures in this article has been generated by Frontiers with the support of artificial intelligence and reasonable efforts have been made to ensure accuracy, including review by the authors wherever possible. If you identify any issues, please contact us.

## Publisher's note

All claims expressed in this article are solely those of the authors and do not necessarily represent those of their affiliated organizations, or those of the publisher, the editors and the reviewers. Any product that may be evaluated in this article, or claim that may be made by its manufacturer, is not guaranteed or endorsed by the publisher.

## References

- Chen, F., and Li, L. (2025). Robust optimization of microgrid and shared energy storage coordination for uncertain scenarios. *Power Syst. Technol.* doi:10.13335/j.1000-3673.pst.2025.0941
- Dong, X., Sun, Y., Malik, S. M., Pu, T., Li, Y., and Wang, X. (2024). Scenario reduction network based on wasserstein distance with regularization. *IEEE Trans. Power Syst.* 39 (1), 4–13. doi:10.1109/TPWRS.2023.3234277
- Dong, H., Wu, L., Zhu, J., Li, S., Liang, Z., Yang, H., et al. (2025). A data-driven cost budget satisficing model for unit commitment under solar power uncertainty. *IEEE Trans. Power Syst.* 40 (5), 4063–4080. doi:10.1109/TPWRS.2025.3543409
- Fu, T., and Fan, C. (2025). Robust collaborative scheduling strategy of multi-microgrid based on non-cooperative game and income distribution mechanism. *Electron. Sci. Technol.* 39 (7). doi:10.16180/j.cnki.issn1007-7820.2026.07.008
- Gao, C., and Zhang, J. (2025). Electricity-heat joint low-carbon scheduling strategy based on Vine copula model and improved ISODATA Clustering. *South. Power Syst. Technol.*
- Gong, J., and Dong, J. (2025). An independent energy storage electricity insurance service model based on asymmetric nash bargaining game. *Mod. Electr. Power* 42, 1–11. doi:10.19725/j.cnki.1007-2322.2024.0065
- Gupta, P. P., Kalkhambkar, V., Kumari, N., Awati, J. S., and Sharma, H. (2025). Optimal scheduling of EV charging station with renewable generation considering line outages and network losses. *IEEE Trans. Industry Appl.* 61 (4), 5626–5636. doi:10.1109/TIA.2025.3545018
- Han, J., Fang, Y., Li, Y., Du, E., and Zhang, N. (2025). Optimal planning of multi-microgrid system with shared energy storage based on capacity leasing and energy sharing. *IEEE Trans. Smart Grid* 16 (1), 16–31. doi:10.1109/TSG.2024.3452064
- Jia, N., Wang, C., Li, Y., Liu, N., and Bi, T. (2025). Robust two-stage dispatch of multi-area integrated electric-gas systems: a decentralized approach. *CSEE J. Power Energy Syst.* 11 (2), 850–860. doi:10.17775/CSEEJPE.2021.04010
- Li, J., and He, X. (2025). Design of peer-to-peer trading for multi-microgrids based on non-cooperative game and distributed machine learning. *Shandong Electr. Power* 50 (312). doi:10.20097/j.cnki.issn1007-9904.2023.11.004
- Li, J., Ma, Y., Gao, J., and Hu, Y. (2025). A Jaya-driven quasi-predictive optimization strategy with adaptive window scheduling for EV thermal management. *Energy* 334, 137593. doi:10.1016/j.energy.2025.137593
- Li, L., Guo, X., and Jing, R. (2025). Optimal scheduling strategy for peak-hour electric vehicles considering effective waiting time and law of delayed gratification. *Electr. Power Syst. Res.* 247, 111739. doi:10.1016/j.epr.2025.111739
- Liang, S., Lou, S., Wu, Y., and Peng, Y. (2024). Generation expansion planning for solvent-stored carbon capture power plants considering the internalization of the carbon emission effects. *IEEE Trans. Power Syst.* 39 (2), 2653–2667. doi:10.1109/TPWRS.2023.3277557
- Lu, Z., Xu, X., Yan, Z., Shahidehpour, M., Sun, W., and Han, D. (2024). Distributionally robust chance constrained optimization method for risk-based routing and scheduling of shared Mobile energy storage system with variable renewable energy. *IEEE Trans. Sustain. Energy* 15 (4), 2594–2608. doi:10.1109/TSTE.2024.3429310
- Luo, W., Yuan, Y., Dong, X., and Wu, H. (2025). Bi-Level optimal dispatching model for EV-Based virtual energy storage system. *CSEE J. Power Energy Syst.* 11 (4), 1556–1569. doi:10.17775/CSEEJPE.2021.07520
- Ma, X., Ning, C., Li, L., Qiu, H., Gu, W., and Dong, Z. (2024). Bayesian nonparametric two-stage distributionally robust unit commitment optimization: from global multimodality to local trimming-wasserstein ambiguity. *IEEE Trans. Power Syst.* 39 (5), 6702–6715. doi:10.1109/TPWRS.2024.3350632
- Malisani, P., Zhu, J., and Pognant-Gros, P. (2023). Optimal charging scheduling of electric vehicles: the Co-Charging case. *IEEE Trans. Power Syst.* 38 (2), 1069–1080. doi:10.1109/TPWRS.2022.3172286
- Mi, Y., Lu, C., Li, C., Qiao, J., Shen, J., and Wang, P. (2025). Data-driven Volt-VAR coordinated scheduling with Mobile energy storage system for active distribution network. *IEEE Trans. Sustain. Energy* 16 (1), 242–256. doi:10.1109/TSTE.2024.3453269
- Mishra, S., and Shaik, A. G. (2024). Stochastic search and rescue method for day ahead economic emission load dispatch under wind uncertainty. *IEEE Access* 12, 92826–92839. doi:10.1109/ACCESS.2024.3418966
- Nie, Y., Li, Z., Zhang, J., Gao, L., Li, Y., and Zhou, H. (2025). Optimal dispatch strategy for a multi-microgrid cooperative alliance using a two-stage pricing mechanism. *IEEE Trans. Sustain. Energy* 16 (1), 174–188. doi:10.1109/TSTE.2024.3449909
- Qi, S., Li, D., Hou, L., Wang, H., Xin, L., Jin, Y., et al. (2025). Two-stage robust optimization considering the uncertainty of sources and loads in virtual power plants. *IEEE Access* 13, 132155–132169. doi:10.1109/ACCESS.2025.3591459
- Satpathy, P. R., Ramachandramurthy, V. K., Krishnan, T. R. R., and Padmanaban, S. (2025). Technological innovations and sustainable strategies for advancing electric vehicle performance and market integration. *Energy Strategy Rev.* 60, 101790. doi:10.1016/j.esr.2025.101790
- Saw, B. K., and Bohre, A. K. (2025). Sustainable deployment of EV charging stations in distribution network supported with hybrid Solar-DG integrated DSTACOM. *IEEE Trans. Industry Appl.* 61 (5), 7750–7765. doi:10.1109/TIA.2025.3550143
- Sui, Q., Zhang, J., Sun, L., Liang, J., Wei, F., and Lin, X. (2024). Optimal scheduling of Mobile energy storage capable of variable speed energy transmission. *IEEE Trans. Smart Grid* 15 (3), 2710–2722. doi:10.1109/TSG.2023.3329294
- Wang, Y., and Zhang, P. (2025). Low-carbon optimal dispatch strategy for microgrid alliance considering Electricity-CCER coupling transaction. *Automation Electr. Power Syst.* doi:10.7500/aeps.20250310008
- Wu, W., Zhu, J., Liu, Y., Luo, T., Chen, Z., and Dong, H. (2024). A coordinated model for multiple electric vehicle aggregators to grid considering imbalanced liability trading. *IEEE Trans. Smart Grid* 15 (2), 1876–1890. doi:10.1109/TSG.2023.3294608
- Zhang, J., Che, L., and Shahidehpour, M. (2023). Distributed training and distributed execution-based stackelberg multi-agent reinforcement learning for EV charging scheduling. *IEEE Trans. Smart Grid* 14 (6), 4976–4979. doi:10.1109/TSG.2023.3309528
- Zhang, T., Chen, C., Ma, L., Chen, T., Wei, Y., Lin, Z., et al. (2024). Multi-step clustering and generalized nash bargaining-based planning strategy of community-shared energy storage for large-scale prosumers. *IEEE Trans. Sustain. Energy* 15 (2), 1013–1027. doi:10.1109/TSTE.2023.3323337